Atomistic Description of Electron Beam Damage in Nitrogen-Doped Graphene and Single-Walled Carbon Nanotubes

Toma Susi,[†,○,*] Jani Kotakoski,[‡,§,○,*] Raul Arenal,[⊥,∥,¶] Simon Kurasch,[#] Hua Jiang,[†] Viera Skakalova,[‡,△] Odile Stephan,[▽] Arkady V. Krasheninnikov,[§,$] Esko I. Kauppinen,[†] Ute Kaiser,[#,*] and Jannik C. Meyer[‡,#]

[†]Nanomaterials Group, Department of Applied Physics, Aalto University School of Science, P.O. Box 15100, 00076 Aalto, Finland, [‡]Department of Physics, University of Vienna, Boltzmanngasse 5, 1090 Vienna, Austria, [§]Department of Physics, University of Helsinki, P.O. Box 43, 00014 University of Helsinki, Finland, [⊥]LMA, Instituto de Nanociencia de Aragon, U. Zaragoza, c/Mariano Esquillor, 50018 Zaragoza, Spain, [∥]Fundacion ARAID, 50004 Zaragoza, Spain, [¶]LEM, UMR 104 CNRS-ONERA, 29 avenue de la Division Leclerc, 92322 Châtillon, France, [#]Central Facility for Electron Microscopy, Group of Electron Microscopy of Materials Science, University of Ulm, 89081 Ulm, Germany, [△]Max Planck Institute for Solid State Research, Heisenbergstrasse 1, 70569 Stuttgart, Germany, [▽]LPS, UMR 8502 CNRS, Université Paris Sud XI, Bâtiment 510, F 91405 Orsay, France, and [$]Department of Applied Physics, Aalto University, P.O. Box 11100, 00076 Aalto, Finland. [○]These authors contributed equally to this work.

ABSTRACT By combining *ab initio* simulations with state-of-the-art electron microscopy and electron energy loss spectroscopy, we study the mechanism of electron beam damage in nitrogen-doped graphene and carbon nanotubes. Our results show that the incorporation of nitrogen atoms results in noticeable knock-on damage in these structures already at an acceleration voltage of 80 kV, at which essentially no damage is created in pristine structures at corresponding doses. Contrary to an early estimate predicting rapid destruction *via* sputtering of the nitrogen atoms, in the case of substitutional doping, damage is initiated by displacement of carbon atoms neighboring the nitrogen dopant, leading to the conversion of substitutional dopant sites into pyridinic ones. Although such events are relatively rare at 80 kV, they become significant at higher voltages typically used in electron energy loss spectroscopy studies. Correspondingly, we measured an energy loss spectrum time series at 100 kV that provides direct evidence for such conversions in nitrogen-doped single-walled carbon nanotubes, in excellent agreement with our theoretical prediction. Besides providing an improved understanding of the irradiation stability of these structures, we show that structural changes cannot be neglected in their characterization employing high-energy electrons.

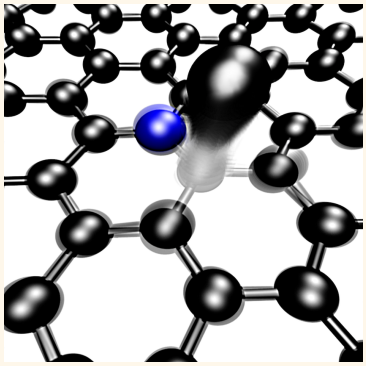

KEYWORDS: graphene · SWCNT · nitrogen doping · DFT · TEM · EELS · irradiation · knock-on damage

It is well-known that sp^2-bonded carbon structures have exceptional physical, chemical, and electrical properties both in the case of two-dimensional graphene[1] and the cylindrical allotrope, single-walled carbon nanotube[2] (SWCNT). However, full realization of their potential for applications is hampered by a lack of control over their electronic structure that was achieved decades ago in conventional semiconductor technology. For SWCNTs, the mixture of semiconducting and metallic tubes[3] in as-grown samples is not acceptable for many applications, while graphene lacks a band gap,[4] leaving graphene devices without an "off" state. Since the early 1990s,[5,6] doping SWCNTs with nitrogen has been considered[7−10] a viable option for tailoring their properties, while nitrogen-doped graphene (N-graphene) has attracted increasing attention more recently.[11−15] Significant electron doping and band gap opening have already been reported for N-graphene,[16] as well as n-type graphene nanoribbon transistors.[17] Nitrogen doping also confers genuinely new properties, such as selective sensitivity for adsorbants[18] and electrochemical catalytic activity.[19−21]

Achieving the desired functionality or modification of host properties depends sensitively on the local bonding configurations of the nitrogen dopants.[7,8,22] The high spectral resolution of X-ray photoelectron spectroscopy (XPS) has revealed the presence of several configurations in nanotube samples.[23,24] As a surface-sensitive method, it has also been popular for studying N-graphene.[11,16,17] At the atomic level, some configurations have been tentatively identified by scanning tunneling microscopy (STM) and spectroscopy.[13,25,26] Unfortunately, such measurements are limited to very small areas, and interpretation of the results remains complicated as different local structures may give rise to similar features. The intermediate spatial resolution offered by electron energy loss spectroscopy (EELS) in transmission electron microscopy (TEM) instruments has been particularly useful for nanotubes,[6,22,27−29] but technical

* Address correspondence to toma.susi@aalto.fi, jani.kotakoski@iki.fi, ute.kaiser@uni-ulm.de.

Received for review June 19, 2012 and accepted September 24, 2012.

Published online September 24, 2012
10.1021/nn303944f

limitations have hitherto not allowed an unambiguous identification of the dopant structures. More recently, cutting-edge developments in instrumentation have enabled atom-by-atom analysis of graphene[30,31] and similar materials[32] and even direct imaging of nitrogen sites.[15] Overall, the latest advances have steadily increased the importance of TEM-based methods.

Although electron beam effects in undoped sp^2-bonded carbon structures have been studied for decades,[33] quantitative analysis on a single-atom level became possible only recently.[34] Earlier estimates were based on atomistic simulations with only qualitative comparisons to experiments, complicated by the fact that different computational methods yielded differing results.[35] Moreover, most simulations gave displacement threshold values higher than experimental estimates, a result attributed to effects associated with electronic excitations neglected in simulations.[35,36] A direct comparison between accurate experiments and simulations solved this discrepancy in the case of graphene.[34] It turned out that lattice vibrations must be taken into account when estimating the displacement cross sections from simulated threshold energies. When this was done, electron irradiation-induced damage in graphene could be completely described by elastic knock-on collisions between the electrons and target atoms in graphene, which lead to atomic displacements with a cross section approximated utilizing the McKinley–Feshbach formula.[37] An excellent agreement was reached with experimental results and simulations without any fitted parameters.[34] This is in line with an earlier estimate that, for example, heating caused by the electron beam during a typical experiment has only a negligible effect on a graphenic target material.[38] The results revised the old assumption of a sharp threshold at acceleration voltages slightly above 80 kV (for sp^2-bonded carbon structures) after which atomic displacements become possible[33] with a smooth onset between ~80 and 110 kV.[34]

However, much less is known about electron irradiation effects in nitrogen-doped structures. So far, the only study on electron beam damage in N-graphene or nitrogen-doped SWCNTs (N-SWCNTs) was carried out with tight-binding simulations[39] and for merely one of the several proposed dopant structures.[7,8] The results suggested a displacement threshold below 14 eV for the nitrogen atom in a substitutional configuration in flat sp^2-bonded carbon, which would lead to a considerable displacement cross section already at an acceleration voltage of 80 kV. Indeed, N-SWCNTs have been found to be significantly less stable than pristine tubes under both 100 and 200 keV electron irradiation.[29] It is also known that irradiation at 100 keV imposes significant changes in the atomic structure of graphenic samples.[38,40] Nevertheless, EELS experiments have been typically performed with dedicated scanning TEM instruments operated at 100 kV (see, refs 6, 22, 27–29, 41, and 42)—or at even higher voltages with energy-filtered TEM devices.[43–45] On the other hand, stable imaging of N-SWCNTs is feasible[42] at 80 kV, which contradicts the simulation result. Furthermore, recent experiments[15] employing aberration-corrected (AC) electron optics for high-resolution TEM (HRTEM) have shown that N-graphene grown by chemical vapor deposition (CVD) remains stable under such conditions for long exposure times and correspondingly high doses. Overall, electron beam effects in nitrogen-doped nanocarbon structures are not sufficiently well-understood to accurately assess the reliability of TEM-based measurements.

RESULTS AND DISCUSSION

In this study, we use *ab initio* molecular dynamics simulations to evaluate the electron irradiation stability of nitrogen-doped graphene and SWCNTs taking into account various proposed local atomic configurations of the dopant sites. Unlike what was previously assumed,[39] our calculations predict that it is substantially easier to displace one of the carbon atoms right next to the nitrogen dopant rather than the dopant itself. Indeed, we directly image these events by 80 kV atomic-resolution AC-HRTEM of N-graphene, which initially shows only nitrogen substitutions, in agreement with previous studies.[11,15,26,46] We also carry out the first quantitative damage analysis for N-SWCNTs from the HRTEM image and EEL spectrum sequences. Our results indicate that, unlike for pristine nanotubes, knock-on damage is the main contributor in the structural failure of N-SWCNTs under an electron beam at 80 kV, although it is obscured by self-healing and reconstructions at room temperature (RT). We also carry out consecutive EELS measurements on the same sample position (chronospectrum mode[47]) to obtain direct spectroscopic evidence for the predicted transformations between the dopant configurations, confirming our simulation results and TEM observations. In general, our results show that structural changes must be considered in any experiments where high-energy electrons are used for probing nitrogen-doped nanocarbons.

DFT Simulations. We started our study by carrying out dynamical atomistic simulations to obtain displacement thresholds (T_D) for the most widely discussed dopant configurations[7,8,18,46,48]—substitutional N, the single (1NV), double (2NV), and triple pyridinic vacancies (3NV), and the quadruple pyridinic divacancy (4ND)—in nitrogen-doped nanocarbons. Due to earlier discrepancies between *ab initio* and tight-binding simulations for noncarbon systems,[35] we used a well-established simulation approach at the DFT level of approximation (the interested reader can find more information on the method in refs 34, 35, 49, and 50 and the references therein). Within this approach, the

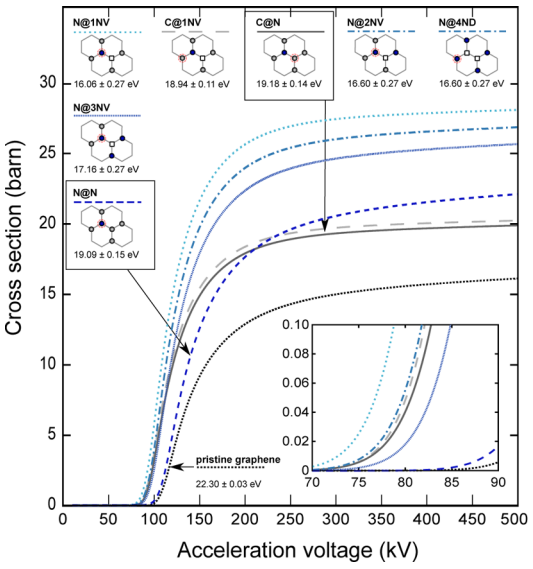

Figure 1. Calculated displacement thresholds and cross sections for different dopant configurations in graphene: substitution (labeled 'N'), single pyridinic vacancy (1NV), double pyridinic vacancy (2NV), triple pyridinic vacancy (3NV), and quadruple pyridinic divacancy (4ND). In the schematic presentations, a dashed red circle marks the atom for which the threshold is calculated. Blue atoms denote nitrogen, gray ones carbon, and vacancies are marked by open squares. The cross sections calculated at RT are shown as a function of the acceleration voltage of the electrons, with the inset showing a higher magnification around 80 kV.

result of an electron−nucleus impact is modeled by assigning a certain kinetic energy to one of the atoms in the structure and then following the time evolution of the system after the impact by DFT molecular dynamics simulations. T_D is defined as the kinetic energy sufficient to displace the atom from its lattice site without an immediate recombination with the resulting vacancy. In the case of low-dimensional structures like graphene and carbon nanotubes, this process is analogous to sputtering in a conventional bulk material. We point out that although static vacancy formation energy calculations can in some cases give reasonable estimates of T_D,[51] this does not work in the general case.[50] Therefore, dynamical simulations remain as the only reliable way to calculate T_D values.

Results of these calculations along with schematic dopant structures are presented in Figure 1. (We point out that our relaxed atomic configurations are in good agreement with the literature, *e.g.*, refs 7, 8, 18, 45, 47, and thus omit here a detailed analysis of the bond lengths and angles which is not relevant for the present study.) We also improved our earlier DFT estimate[35] for the T_D in pristine graphene and obtained a value of 22.30 eV. All of the presented T_D values are calculated for a displacement orthogonal to the graphene membrane and for an atomically flat structure. We point out that our result for the substitutional nitrogen dopant (19.09 eV) differs considerably from the earlier estimate (<14 eV) obtained with a tight-binding method.[39] In fact, none of our calculated T_D values were below 16 eV. However, this discrepancy is in line with the lower T_D values predicted with a similar tight-binding model for hexagonal BN monolayers[36] as compared to more accurate DFT calculations.[35]

After knowing T_D, one can estimate the corresponding displacement cross section (σ) using the McKinley−Feshbach approximation,[33,37] taking into account the lattice vibrations which have a significant contribution to the energy transferred from an electron to the nucleus.[34] We assume a velocity distribution for the target atoms based on the Debye model with a Debye temperature of 1287 K.[52] Note that the mass and the atomic number Z difference of the C and N atoms lead to different σ even when the T_D values are similar. The calculated σ values are plotted along the T_D in Figure 1 for a wide range of electron energies or, correspondingly, acceleration voltages (0−500 kV).

These values can be directly used to estimate the relative stability of different atomic configurations under an electron beam, such as during TEM imaging or an EEL spectrum acquisition. For example, in the case of substitutional doping, the cross section for displacing the carbon atom next to the dopant (C@N) is higher than that for displacing the dopant itself (N@N) up to acceleration voltages of >200 kV. The actual difference in sputtering probabilities is even larger because there are three C@N for each N@N. This tendency is universal among all of the defects; although some of the dopant atoms have higher cross sections than the neighboring carbon atoms, since there are always more of them, sputtering one of the carbon atoms is more likely. Therefore, for any of the dopant configurations, the atomic structure of the dopant site is likely to be changed by displacing a carbon atom before the dopant atom itself is sputtered under electron irradiation.

N-Graphene Experiments. Our previous studies suggest a good agreement for pristine graphene between calculated T_D values and experiments.[34] To confirm the present simulation results, we imaged CVD-grown[53] N-graphene at 80 kV using high irradiation doses both to obtain a high signal-to-noise ratio and to estimate the displacement cross section of the dopant configurations in this material. The N-graphene samples had regions of monolayer and few-layer graphene,[15,53] as is typical for CVD-grown graphene on Cu. Only free-standing monolayer areas, identified by their appearance in high-resolution TEM images[54] and further confirmed by the step edges to vacuum areas visible in Figures 2 and 3, were considered for the present study. For our analysis, we selected clean areas of the graphene membranes, free of defects or contamination.

As we have shown previously,[15] contrary to the widely used independent atom model,[55] atomic potentials derived from all-electron DFT calculations

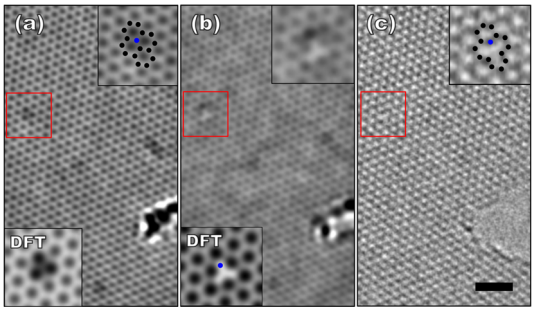

Figure 2. Electron micrographs of N-graphene recorded at 80 kV (FEI Titan 80-300). The top right insets in each panel show an enlarged view of the area marked by the red square (N atom denoted by a blue and C atoms by black full circles). (a) Area of undamaged N-graphene. Three darker bonds around a central atom reveal the positions of the substitutional N dopants,[15] five of which are in the field of view. The bottom left inset shows a DFT image simulation[57] of a N substitution at a corresponding defocus. (b) Same area after a cumulative electron dose of 1.9×10^7 $e^-/Å^2$. The change of contrast at the site corresponds to a missing atom displaced by an electron impact. The bottom left inset shows the simulation of the single pyridinic vacancy (1NV) defect (the position of the two-coordinated N atom marked by the blue full circle at the reconstructed vacancy), exhibiting the triangular contrast seen in the experimental image. (c) Unprocessed image of the same area at the Scherzer defocus, allowing a direct interpretation of the atomic structure and revealing more clearly the 5−9 vacancy next to the nitrogen atom (that is, the 1NV). All images were recorded with spherical aberration values around 20 μm. Those in panels (a) and (b) are averages of several exposures recorded with a defocus of −18 nm to enhance the contrast of the N dopants,[15] while panel (c) was recorded at the Scherzer defocus (−9 nm). The scale bar is 1 nm.

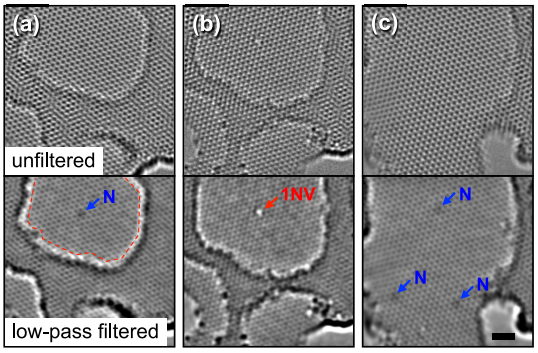

Figure 3. Observations from a long HRTEM image sequence of N-graphene. The top row shows unfiltered images (averages of 20−30 subsequent exposures), while the bottom row shows the same images with a low-pass filter applied.[15] The red dashed line in (a) indicates a monolayer region surrounded by a bilayer area; this monolayer grows during the experiment. The substitutional N atom (marked by a blue arrow in a) is converted into the single pyridinic vacancy (1NV, red arrow, b), and then subsequently back to a nitrogen substitution (c). In (c), two additional N atoms previously under the monolayer−bilayer interface have become visible. The scale bar is 1 nm.

show that electron scattering on the carbon atom next to a nitrogen differs appreciably from electron scattering on a carbon atom elsewhere in the graphene sheet. Thus N substitutions can be directly detected in correctly defocused TEM images as three darker bonds surrounding a central atom, identified as nitrogen by DFT image simulations. This methodology is described in detail in ref 15.

In the beginning of the imaging experiments, all observed nitrogen atoms were in the substitutional configuration. On the basis of earlier theoretical work,[39] under our 80 kV imaging conditions, one should expect a cross section of more than 2 barn for displacing one such nitrogen dopant (taking into account lattice vibrations[34]). In one of our experiments with a dose up to 2.5×10^7 $e^-/Å^2$, we had eight substitutional nitrogen sites in the field of view simultaneously in an area of approximately 240 nm^2, in good agreement with the 0.1 atom % substitutional doping level determined previously by statistical TEM observations of the material.[53] (Two dopants were third nearest neighbors, similar to a configuration that has been tentatively detected recently by STM.[13]) A cross section of ~2 barn would lead to displacing at least one of the N atoms at a dose roughly one-fifth of the maximum dose used. By contrast, none of the N atoms were sputtered by the end of any of our experiments, validating the low cross section calculated based on our DFT simulation results (Figure 1). However, we observed another change in the atomic structure of the dopant sites during imaging. An example of a particularly nitrogen-rich area (with approximately 0.4 atom % N concentration locally) is presented in Figure 2.

From Figure 2, it can be directly seen that, instead of the dopant atom, the first atom displaced by the electron beam is one of the three carbon atoms next to it, in agreement with our calculations. In the resulting atomic configuration, the nitrogen atom remains two-coordinated whereas the two undercoordinated carbon atoms bond, forming a pentagon (the 1NV configuration).[56] Although our TEM observations did not reveal the 1NV prior to electron beam damage, the stability of the structure immediately after its appearance indicates that it is at least a metastable configuration in graphene. In nanotubes, curvature should further increase its thermodynamical stability.[18,45]

By the end of this experiment, three of the eight N substitutions had been converted into 1NV in and around the area shown in Figure 2. In total, we observed five conversions of the 35 imaged sites during our experiments up to doses ~2.5×10^7 $e^-/Å^2$. This data set allows us to make a statistical estimate for the upper limit of the displacement cross section of the ejected carbon atoms, resulting in 0.16 barn, which can be directly compared with our calculation result of about 0.03 barn (Figure 1). When we take into account inaccuracies resulting from experimental uncertainties as well as the sensitivity of the theoretical cross section calculations at small values, this can be considered a good agreement. Another point to consider is that, due to the high computational cost of dynamical DFT

simulations, we could only consider displacements in the direction perpendicular to the graphene plane. This may also contribute to the discrepancy since non-orthogonal displacements of atoms with neighbors of different mass may have lower thresholds, unlike atoms in pristine graphene.[49] We also note that, in one of our experiments, a vacancy created during imaging was refilled (Figure 3). This both offers direct evidence for defect healing *via* adatom migration in our RT experiments as well as shows that it remains slow enough to be captured by atomic-resolution imaging.

Effect of Curvature. As mentioned above, it was not feasible to extend our calculations to other displacement directions or curved structures. Fortunately, the effects of curvature of the structure[39,58,59] as well as the displacement direction[36,38,49] are relatively well-understood based on previous studies. For example, it is known that for a diameter of $d \sim 2$ nm, the values of T_D approach those of graphene but decrease with increased curvature for smaller nanotubes. Also, atoms in the "sides" of nanotubes (with respect to the electron beam) are known to have much larger thresholds.[38] As doping is likely inhomogeneous but isotropic on average, we estimate that 50% of dopant sites have thresholds close to those we calculated.[38] Displacements of these atoms, located at the "top" and "bottom" of the tube should dominate the apparent σ in SWCNT experiments.

To take into account the curvature effect in N-SWCNTs, we have fitted an empirical function to describe the diameter dependency of T_D (Figure 4) using available literature data.[39,58,59] Employing this function, we estimate the expected thresholds for nanotubes with different diameters from values calculated for graphene. Table 1 lists the values for the dopant configurations presented in Figure 1 as well as for single and double vacancies in undoped structures. We also present the calculated σ for each configuration either at −100 °C and 80 kV or at RT and 100 kV to facilitate comparison with experiments presented below.

N-SWCNT Experiments. Since only nitrogen substitutions were detected in our N-graphene samples, we expanded the study to N-SWCNTs, where pyridinic configurations are expected to be important.[8,18] Especially the 3NV and 4ND configurations[8,18] should be attractive targets for direct imaging because the presence of the N atoms causes the relaxation of the pyridinic structures[18] to be different from the pristine reconstructed single (5-9) or double (5-8-5) vacancies.[60,61] However, TEM experiments with SWCNTs are inherently more challenging than with graphene, partly because SWCNT samples are less stable mechanically, which tends to limit achievable resolution. Moreover, the two-dimensional projection image of the curved surface makes the interpretation of structure more challenging. Finally, even at room temperature, adatom diffusion,[62] particularly inside the tubes, can anneal damage[49] before it can be observed. At least partially due to these limitations, the resolution in our N-SWCNT experiments did not allow us to directly image the nitrogen dopants; the required combination of excellent stability, high vacuum, sample quality, and microscope

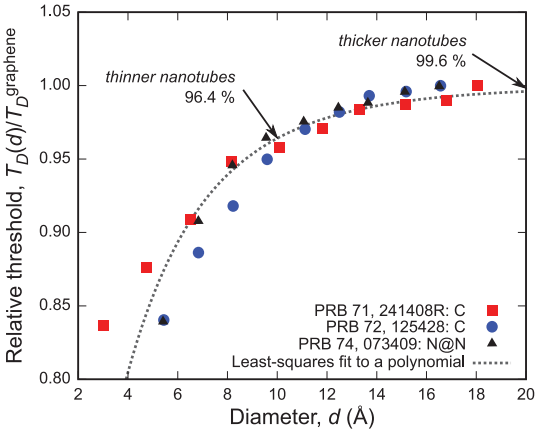

Figure 4. Relative displacement threshold values taken from the literature as a function of nanotube diameter. Fitting a polynomial (dotted line) into the data shows that the threshold for a 1 nm nanotube is about 96.4% of the graphene value, whereas for a 2 nm one, it is about 99.6%. The values for carbon[58,59] (C, squares and circles) were calculated for pristine SWCNTs, while those for nitrogen[39] (N, triangles) correspond to N substitutions (N@N).

TABLE 1. Influence of SWCNT Diameter (Fitted According to Figure 4) on the Displacement Thresholds of Carbon or Nitrogen Atoms for Different Atomic Configurations (Figure 1)

target[a]	d (nm)	T_D (eV)	$\sigma_{80kV}^{-100°C}$ (barn)	σ_{100kV}^{RT} (barn)
C@N	1	18.5	0.08	4.70
	2	19.1	0.03	3.31
N@N	1	18.4	6.5×10^{-4}	0.75
	2	19.0	1.2×10^{-4}	0.36
C@1NV	1	18.3	0.11	5.23
	2	18.9	0.04	3.74
N@1NV	1	15.5	0.31	8.08
	2	16.0	0.13	6.01
N@2NV	1	16.0	0.13	6.01
	2	16.5	0.05	4.29
N@3NV	1	16.5	0.05	4.29
	2	17.1	0.01	2.68
N@4ND	1	16.0	0.13	6.01
	2	16.5	0.05	4.29
C[b]	1	21.5	1.3×10^{-4}	2.4×10^{-4}
	2	22.2	2.0×10^{-5}	4.2×10^{-5}
C@SV[b]	1	14.2	7.43	21.9
	2	14.6	9.58	19.7
C@DV[b]	1	15.6	3.41	14.9
	2	16.1	2.12	12.8

[a] Target atom @ dopant configuration; SWCNT diameter for threshold fitting d; calculated displacement threshold T_D; cross sections (σ) at 80 kV (calculated at −100 °C) and 100 kV (at RT). [b] C, C@SV, and C@DV correspond to C atoms in ideal sp^2-bonded carbon and single and double vacancy configurations, respectively. The T_D values for C@SV and C@DV in graphene are from ref 50.

resolution are not yet available. Nonetheless, since quantitative studies of electron beam damage in N-SWCNTs have not been reported before, these experiments still allow us to obtain useful information complementary to the N-graphene ones and to establish dose control guidelines for future studies.

The N-SWCNT samples were synthesized by floating catalyst CVD as described previously in refs 41 and 42. Pristine SWCNTs were obtained with the same method, but without added ammonia. First, we imaged N-SWCNTs at 80 kV at room temperature with various electron irradiation doses. Although no localized lattice damage was observed, a narrowing of the tube diameter around the beam center was consistently seen at doses on the order of 10^7 e$^-$/Å^2 (Figure 5). We attribute this to the reconstruction of the damaged structures due to thermally activated migration-mediated self-healing (active at room temperature at time scales faster than our imaging[62]) combined with the creation of reconstructed multivacancies,[63] which eventually leads to the observed shrinkage.

Although it is challenging to discern the contributions of different effects in the shrinkage of the nanotubes under electron irradiation, measuring the relative diameter reduction as a function of the irradiation dose allows us to estimate an apparent σ, which includes contributions from all processes (*e.g.*, knock-on damage, healing, reconstruction). In Figure 5, we plot the diameters of three nanotubes with different initial sizes (2.2, 1.8, and 1.4 nm) as a function of irradiation dose. The corresponding apparent cross sections obtained from these data are 0.2, 0.5, and 1.1 barn, respectively. Hence, the overall result is in agreement with the decreasing T_D (and correspondingly increasing σ; see Table 1) with decreasing diameter, as shown in Figure 4. Also, the values themselves are in the expected range, taking into account that a significant number of the sputtered atoms were presumably three-coordinated in reconstructed vacancy configurations, which we expect to have σ in the order of 1 barn (that is, similar to or lower than that of C@DV).

Since decreasing temperature from RT to −100 °C should effectively stop adatom migration (for a barrier of 0.25 eV,[62] the estimated migration rate decreases by 3 orders of magnitude) and limit temperature-assisted reconstructions which lead to the tube shrinkage, we expected that primary damage would become visible by using a cryo-TEM holder. In addition, *via* hindered self-healing, this should elucidate the effects of initial knock-on impacts. Therefore, we performed 80 kV TEM experiments also at −100 °C on both N-doped and pristine SWCNTs. Although cooling the samples seemed to increase the amount of adsorbates on the tubes, we nevertheless observed clear differences in the radiation damage of these structures. For N-SWCNTs, clear signs of damage occurred at doses similar to those required for damaging N-graphene (~1×10^7 e$^-$/Å^2)

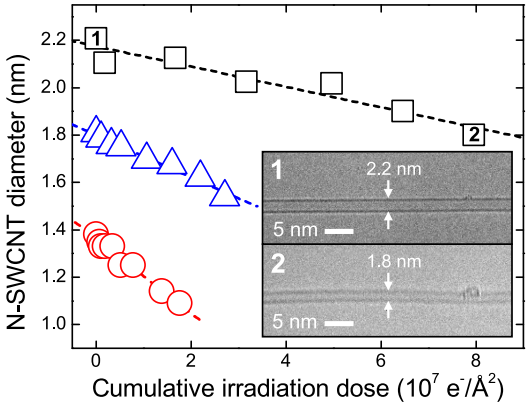

Figure 5. Reduction of N-SWCNT diameter at the center of the 80 kV electron beam measured from the separation of the line profile intensity minima in TEM micrographs of different diameter tubes as a function of the cumulative irradiation dose. The inset shows TEM micrographs (JEOL JEM-2200FS) of the N-SWCNT marked by the numbered black squares in the main graph (1) initially (diameter 2.2 nm) and (2) after a total electron irradiation dose of 7.8×10^7 e$^-$/Å^2 (diameter reduced to ~1.8 nm). Apart from slight curvature, no clear signs of damage were observed during the transformation. We note that the determined diameters are approximate since charging and/or vibrations caused by the continuous irradiation resulted in a loss of resolution, as seen in inset 2.

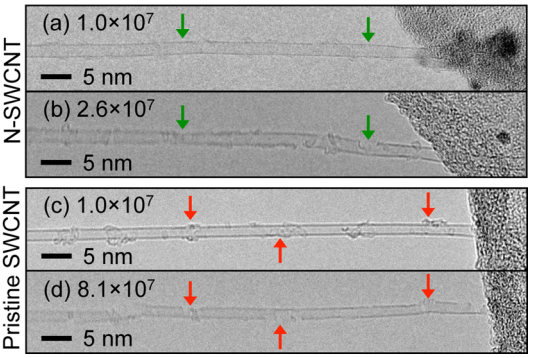

Figure 6. Representative TEM micrographs (JEOL JEM-2200FS) of (a,b) doped and (c,d) pristine SWCNT both with diameters around 2 nm, imaged at 80 kV and −100 °C after the cumulative irradiation doses (in units of e$^-$/Å^2) noted in the images. The top panels for each case (a,c) were recorded after a similar dose (~1.0×10^7 e$^-$/Å^2), while the bottom panels (b,d) were the last images that could be captured before the tubes in question broke down. In the beginning of the experiments, both SWCNTs appeared straight with no visible defects. The green arrows in (a,b) mark areas on the N-SWCNT where no adsorbates are visible, yet which show heavy localized damage after further irradiation. The red arrows in (c,d), by contrast, mark sections of the pristine SWCNT with visible adsorbates where localized damage occurred at higher doses.

(Figure 6a,b), whereas pristine tubes tolerated several times higher doses in otherwise identical conditions (the microscope vacuum was 6.5×10^{-6} Pa in both cases), leading us to attribute this difference to increased knock-on damage in the doped tubes. The results were qualitatively similar for both small (1.1 nm) and large (~2 nm) diameter tubes.

We first point out that, according to our calculations, the observed damage in pristine tubes (Figure 6) appears too fast to be attributable to a knock-on process in a perfect structure (which has $\sigma \sim 10^{-4}$ barn; see Table 1). Moreover, the damage in pristine tubes tends to appear at sites with visible adsorbants (Figure 6c,d), which suggests an active chemical etching process.[34] On the other hand, the damage in N-SWCNTs is slower than what would be expected if there had been a significant number of dopant atoms occupying 1NV sites under the irradiated areas. Although the σ values for N@1NV and C@1NV are roughly similar to that of C@N, the σ calculated for two-coordinated C atoms at a vacancy site—similar to those next to the a 1NV—is 2 orders of magnitude higher. However, the results are consistent with knock-on damage for dopant sites with any of the configurations that have no under-coordinated carbon atoms (*i.e.*, substitutional N, 3NV, or 4ND).

Our −100 °C results also show that larger diameter (~2 nm) SWCNTs tolerate about 40% higher doses than 1.1 nm ones regardless of whether they were doped, in qualitative agreement with the RT results (Figure 5). Moreover, the results are in quantitative agreement with the calculated σ shown in Table 1 (taking into account that the larger tubes have twice the cross sectional area of the smaller ones). Together with the absolute σ values pointing to non-1NV dopant sites, this is a clear indication that knock-on damage leads to structural changes in N-SWCNTs at 80 kV.

EELS Experiments. Finally, having established the role of knock-on damage with our N-SWCNT irradiation experiments, we turn to EELS measurements carried out at the typical voltage of 100 kV.[22,27−29,41,42] Previous studies have detected at least two kinds of doping configurations (substitutional and pyridinic) in N-SWCNTs.[22−24,29] As we have shown above, an electron beam can transform substitutional sites into pyridinic ones at 80 keV. This is particularly important for EELS as the sites have different EELS signatures,[22,64] and such conversions are significantly more likely at the higher acceleration voltage of 100 kV (see Figure 1).

Although the doses were not estimated in our previous work, care was taken to limit the total exposure time. Reanalyzing the published data,[22,41,42] we estimate that the maximum doses used were ~1×10^6 $e^-/Å^2$. On the basis of our simulation results, this would correspond to changing the local atomic structure of up to 3% of substitutional dopant sites into pyridinic ones in N-SWCNTs with $d \approx 1$ nm (using σ from Table 1 and taking into account that each site has three C neighbors). Such a low conversion probability is unlikely to result in a noticeable difference in the recorded spectra. However, we point out that these issues have not been explicitly considered nor doses reported in the literature.

Therefore, to study in detail the changes imposed by electron irradiation, we carried out a time-resolved EELS experiment with a higher dose using a scanning transmission electron microscope (STEM, VG-HB501) equipped with a cold field emission gun operated at 100 kV. For these measurements, we used N-SWCNTs synthesized previously by laser vaporization,[22] which have less adsorbants and slightly better crystallinity than our CVD-synthesized N-SWCNTs. The results are presented in Figure 7. The location where the EEL spectrum was collected (see Figure 7a) contained a small bundle of clean N-SWCNTs (around 1.4 nm in diameter). The energy loss near-edge feature of the C K-edge (Figure 7b) consists of a π^* peak at ~285 eV and a well-defined σ^* band starting at ~292 eV, suggesting high crystallinity of the graphitic walls. An enlargement of the N K-edge after background subtraction is shown in Figure 7c. The contribution at ~399 eV can

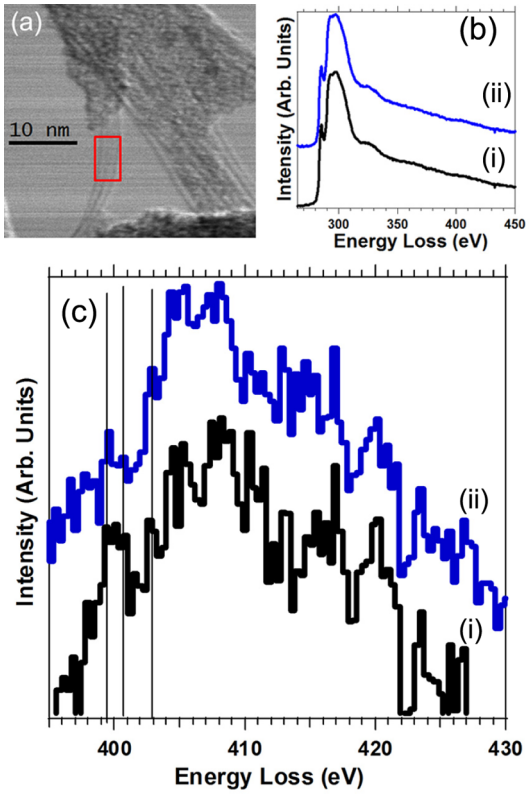

Figure 7. (a) Bright-field micrograph of N-SWCNT material synthesized *via* laser vaporization.[22] EEL spectra were continuously recorded by rastering a defocused beam on the area marked by the red open rectangle during the experiment (each spectrum with an acquisition time of 2.8 s). (b) To obtain a high enough signal-to-noise ratio, we have summed up the first 20 spectra to obtain the black curve, whereas the blue one is a sum of the following 20 spectra. Both display a C K-edge characteristic for SWCNTs. The irradiation dose was approximately 0.45 × 10^7 $e^-/Å^2$ for each sum spectrum. (c) Magnification of the N K-edge after background subtraction. The contribution from substitutional nitrogen dopants (~401 eV) is significantly decreased in the blue spectrum collected with the higher cumulative dose. Interestingly, there seems to also be contributions at ~403 and ~406 eV that would match the core levels of pyridine-*N*-oxide and C-NO_2, respectively.[66] These interesting features should be investigated in more detail in future studies.

be assigned to pyridinic nitrogen, while the one at ~401 eV is due to substitutional nitrogen.[7,22,29] After continuing irradiation to obtain the blue spectrum (cumulative dose around 0.9×10^7 $e^-/Å^2$), the substitutional contribution is significantly reduced. Furthermore, the relative total concentration of nitrogen is slightly increased (from 0.7 to 0.9 atom %), while the concentration of carbon is decreased (from 96.5 to 96.0 atom %). These findings are consistent with sputtering of carbon atoms from sites neighboring nitrogen substitutions in the N-SWCNTs, initially transforming them into pyridinic configurations as predicted by our simulations and directly observed in N-graphene.

Clearly, to avoid misidentifying the dopant structures of the pristine material, it is imperative to either carefully limit the dose or make sure the spectrum time series shows no changes during an EELS experiment. Alternatively, the primary beam energy of the microscope should be 60 kV[30,31] or below.[65]

CONCLUSIONS

Our dynamical density functional theory simulations show that the dominant knock-on mechanism in nitrogen-doped graphene and SWCNTs initiates by first displacing a carbon atom next to a substitutional nitrogen dopant, not the nitrogen atom itself as was previously assumed. Since N-graphene tolerates high irradiation doses at 80 kV, we were able to directly observe this process by AC-HRTEM imaging and to establish a reasonably good agreement between our theoretically obtained displacement cross section values and the estimate based on experimental data. We further used the simulation results to estimate the stability of several proposed nitrogen dopant sites in SWCNTs. By carrying out experiments both at room temperature and at −100 °C, we demonstrated that knock-on damage in N-SWCNTs at room temperature is partially obscured by self-healing and reconstruction of the nanotube walls, which can lead to an overestimation of the stability of these structures. The reduced temperature experiments showed that N-SWCNTs tolerate several times lower doses than pristine nanotubes, in agreement with the increased displacement cross sections at the dopant sites. Finally, in agreement with our simulations and TEM experiments, we obtained direct spectroscopic evidence for conversions of substitutional dopant configurations into pyridinic ones in N-SWCNTs by EELS time series measurement carried out at 100 kV. Overall, our results highlight the importance of taking into account the structural changes imposed by energetic electrons on doped carbon nanomaterials even when pristine structures are known to remain unchanged under similar conditions.

METHODS

Simulations. For the threshold calculations, we used density functional theory as implemented in the VASP simulation package.[67,68] Core electrons were described with projector-augmented wave potentials,[69] and exchange and correlation was estimated by the generalized gradient approximation.[70] For our dynamical simulations, we used a Monkhorst-Pack *k*-point mesh[71] of $5 \times 5 \times 1$. The system consisted of an 8×6 supercell with 96 atoms and 10 Å of empty space between the periodic images. We used a kinetic energy cutoff of 300 eV.

The TEM image simulations were based on projections of the electrostatic potential corresponding to the all-electron self-consistent electron density from the WIEN2k DFT code[72] as described in ref 57.

N-Graphene. Nitrogen-doped graphene was synthesized[15,53] on Cu substrates with ammonia as the doping agent and methane as the carbon precursor, following the CVD method described in ref 11. The substitutional N doping level was determined to be 0.1 atom % by statistical TEM observations.[53] The N-graphene sheets were transferred onto TEM grids as previously explained.[73]

N-SWCNTs. Nitrogen-doped single-walled carbon nanotubes were grown from ferrocene-derived iron nanoparticles by a floating catalyst CVD method[41,42] with ammonia as the doping agent and carbon monoxide as the carbon precursor. The doping concentration of samples synthesized with this method was previously determined to be in the range of 0.1 to 1%[41,42] and is expected to be inhomogeneous.[74] Pristine SWCNTs were obtained with the same procedure, but without added ammonia. The N-SWCNTs were collected onto TEM grids directly from the gas phase using an electrostatic precipitator corona charger.[75] Additional N-SWCNTs for EELS experiments were previously synthesized by laser vaporization of a graphite target mixed with Ni/Y catalyst powders in a 300 mbar N_2 atmosphere.[22]

TEM Experiments. The N-graphene samples were irradiated using an imaging-side aberration-corrected FEI Titan 80-300 operated at 80 kV. For enhancing the N atom contrast, a defocus of −18 nm was used and the graphene lattice contrast suppressed by applying a low-pass filter to averages of 30−40 exposures as described in ref 15. The SWCNT samples were irradiated using a double aberration-corrected JEOL JEM-2200FS operated at 80 kV. Before observation, the nanotube samples were heated at 150 °C for at least 30 min to clean the sample surfaces of some adsorbates. For the reduced temperature experiments, the samples were cooled to −100 °C inside the microscope using a Gatan 914 nitrogen-cooled cryotransfer holder.

EELS Experiments. Electron energy loss spectra were recorded using a VG-HB501 scanning TEM equipped with a cold field emission gun, operated at 100 keV with an energy resolution of 0.7−0.8 eV in the core-loss region. The convergence angle on the sample and collection angle of the spectrometer were 15 and 24 mrad, respectively. The spectroscopic information was obtained using the spectrum-imaging acquisition mode,[64,76] with a slightly defocused electron probe scanned in an area of a few square nanometers. Principal components analysis (PCA) was used for analyzing and denoising the EELS data. This treatment confirms that, considering the experimental signal-to-noise ratio and energy resolution, the spectral contributions around 399−401 eV in Figure 7 can be decomposed into two main components of changing weight as a function of the electron dose.

Conflict of Interest: The authors declare no competing financial interest.

Acknowledgment. We are grateful to Hye Jin Park for her work on the synthesis of the N-graphene samples, and to Annick Loiseau for useful discussions. We also acknowledge Nathalie Brun for her assistance with the PCA analysis. T.S. received support from the Finnish Foundation for Technology Promotion. T.S., H.J., and E.I.K. further acknowledge financial support from the CNB-E project of the Aalto MIDE program and from the

LiBaCAM project of TEKES. J.K. and A.V.K. acknowledge financial support from Helsinki University Funds and Academy of Finland through several projects as well as CSC Ltd. Finland for computational resources. S.K., U.K., and J.C.M. acknowledge the financial support by the DFG (German Research Foundation) and the Ministry of Science, Research and the Arts (MWK) of Baden-Wuerttemberg in the frame of the SALVE (Sub Angstrom Low-Voltage Electron microscopy) project. V.S. acknowledges an EC Grant No. 266391 related to the project ELECTROGRAPH (FP7/2007-2013).

REFERENCES AND NOTES

1. Geim, A. K.; Novoselov, K. S. The Rise of Graphene. *Nature Mater.* **2007**, *6*, 183–191.
2. Dresselhaus, M. S.; Dresselhaus, G.; Avouris, P. *Carbon Nanotubes: Synthesis, Structure, Properties and Applications*; Springer: Berlin, 2001.
3. Saito, R.; Dresselhaus, G.; Dresselhaus, M. S. Trigonal Warping Effect of Carbon Nanotubes. *Phys. Rev. B* **2000**, *61*, 2981.
4. Castro Neto, A. H.; Guinea, F.; Peres, N. M. R.; Novoselov, K. S.; Geim, A. K. The Electronic Properties of Graphene. *Rev. Mod. Phys.* **2009**, *81*, 109–162.
5. Yi, J. Y.; Bernholc, J. Atomic Structure and Doping of Microtubules. *Phys. Rev. B* **1993**, *47*, 1708–1711.
6. Stephan, O.; Ajayan, P. M.; Colliex, C.; Redlich, P.; Lambert, J. M.; Bernier, P.; Lefin, P. Doping Graphitic and Carbon Nanotube Structures with Boron and Nitrogen. *Science* **1994**, *266*, 1683.
7. Ewels, C. P.; Glerup, M. Nitrogen Doping in Carbon Nanotubes. *J. Nanosci. Nanotechnol.* **2005**, *5*, 1345–1363.
8. Ayala, P.; Arenal, R.; Loiseau, A.; Rubio, A.; Pichler, T. The Physical and Chemical Properties of Heteronanotubes. *Rev. Mod. Phys.* **2010**, *82*, 43.
9. Ayala, P.; Arenal, R.; Rümmeli, M. H.; Rubio, A.; Pichler, T. The Doping of Carbon Nanotubes with Nitrogen and Their Potential Applications. *Carbon* **2010**, *48*, 585–586.
10. Arenal, R.; Blase, X.; Loiseau, A. Boron-Nitride and Boron-Carbonitride Nanotubes: Synthesis, Characterization and Theory. *Adv. Phys.* **2010**, *59*, 101–179.
11. Wei, D.; Liu, Y.; Wang, Y.; Zhang, H.; Huang, L.; Yu, G. Synthesis of N-Doped Graphene by Chemical Vapor Deposition and Its Electrical Properties. *Nano Lett.* **2009**, *9*, 1752–1758.
12. Janowska, I.; Chizari, K.; Ersen, O.; Zafeiratos, S.; Soubane, D.; Costa, V.; Speisser, V.; Boeglin, C.; Houllé, M.; Bégin, D.; Plee, D.; Ledoux, M.-J.; Pham-Huu, C. Microwave Synthesis of Large Few-Layer Graphene Sheets in Aqueous Solution of Ammonia. *Nano Res.* **2010**, *3*, 126–137.
13. Deng, D.; Pan, X.; Yu, L.; Cui, Y.; Jiang, Y.; Qi, J.; Li, W.-X.; Fu, Q.; Ma, X.; Xue, Q.; Sun, G.; Bao, X. Toward N-Doped Graphene *via* Solvothermal Synthesis. *Chem. Mater.* **2011**, *23*, 1188–1193.
14. Åhlgren, E. H.; Kotakoski, J.; Krasheninnikov, A. V. Atomistic Simulations of the Implantation of Low-Energy Boron and Nitrogen Ions into Graphene. *Phys. Rev. B* **2011**, *83*, 115424.
15. Meyer, J. C.; Kurasch, S.; Park, H. J.; Skakalova, V.; Künzel, D.; Gross, A.; Chuvilin, A.; Algara-Siller, G.; Roth, S.; Iwasaki, T.; Starke, U.; Smet, J. H.; Kaiser, U. Experimental Analysis of Charge Redistribution Due to Chemical Bonding by High-Resolution Transmission Electron Microscopy. *Nature Mater.* **2011**, *10*, 209–215.
16. Usachov, D.; Vilkov, O.; Grüneis, A.; Haberer, D.; Fedorov, A.; Adamchuk, V. K.; Preobrajenski, A. B.; Dudin, P.; Barinov, A.; Oehzelt, M.; Laubschat, C.; Vyalikh, D. V. Nitrogen-Doped Graphene: Efficient Growth, Structure, and Electronic Properties. *Nano Lett.* **2011**, *11*, 5401–5407.
17. Wang, X.; Li, X.; Zhang, L.; Yoon, Y.; Weber, P. K.; Wang, H.; Guo, J.; Dai, H. N-Doping of Graphene through Electrothermal Reactions with Ammonia. *Science* **2009**, *324*, 768–771.
18. Rocha, A.; Rossi, M.; Silva, A.; Fazzio, A. Realistic Calculations of Carbon-Based Disordered Systems. *J. Phys. D: Appl. Phys.* **2010**, *43*, 374002.
19. Gong, K.; Du, F.; Xia, Z.; Durstock, M.; Dai, L. Nitrogen-Doped Carbon Nanotube Arrays with High Electrocatalytic Activity for Oxygen Reduction. *Science* **2009**, *323*, 760–764.
20. Qu, L.; Liu, Y.; Baek, J.-B.; Dai, L. Nitrogen-Doped Graphene as Efficient Metal-Free Electrocatalyst for Oxygen Reduction in Fuel Cells. *ACS Nano* **2010**, *4*, 1321–1326.
21. Machado, B. F.; Serp, P. Graphene-Based Materials for Catalysis. *Catal.: Sci. Technol.* **2012**, *2*, 54–75.
22. Lin, H.; Arenal, R.; Enouz-Vedrenne, S.; Stephan, O.; Loiseau, A. Nitrogen Configuration in Individual CN_x-SWCNTs Synthesized by Laser Vaporization Technique. *J. Phys. Chem. C* **2009**, *113*, 9509–9511.
23. Ayala, P.; Gruneis, A.; Gemming, T.; Grimm, D.; Kramberger, C.; Rummeli, M. H.; Freire, F. L., Jr.; Kuzmany, H.; Pfeiffer, R.; Barreiro, A. Tailoring N-Doped Single and Double Wall Carbon Nanotubes from a Nondiluted Carbon/Nitrogen Feedstock. *J. Phys. Chem. C* **2007**, *111*, 2879.
24. Elías, A. L.; Ayala, P.; Zamudio, A.; Grobosch, M.; Cruz-Silva, E.; Romo-Herrera, J. M.; Campos-Delgado, J.; Terrones, H.; Pichler, T.; Terrones, M. Spectroscopic Characterization of N-Doped Single-Walled Carbon Nanotube Strands: An X-ray Photoelectron Spectroscopy and Raman Study. *J. Nanosci. Nanotechnol.* **2010**, *10*, 3959–3964.
25. Czerw, R.; Terrones, M.; Charlier, J. C.; Blase, X.; Foley, B.; Kamalakaran, R.; Grobert, N.; Terrones, H.; Tekleab, D.; Ajayan, P. M.; Blau, W.; Ruhle, M.; Carroll, D. L. Identification of Electron Donor States in N-Doped Carbon Nanotubes. *Nano Lett.* **2001**, *1*, 457–460.
26. Zhao, L.; He, R.; Rim, K. T.; Schiros, T.; Kim, K. S.; Zhou, H.; Gutiérrez, C.; Chockalingam, S. P.; Arguello, C. J.; Pálová, L.; Nordlund, D.; Hybertsen, M. S.; Reichman, D. R.; Heinz, T. F.; Kim, P.; Pinczuk, A.; Flynn, G. W.; Pasupathy, A. N. Visualizing Individual Nitrogen Dopants in Monolayer Graphene. *Science* **2011**, *333*, 999–1003.
27. Terrones, M.; Terrones, H.; Grobert, N.; Hsu, W. K.; Zhu, Y. Q.; Hare, J. P.; Kroto, H. W.; Walton, D. R. M.; Kohler-Redlich, P.; Ruhle, M.; Zhang, J. P.; Cheetham, A. K. Efficient Route to Large Arrays of CN_x Nanofibers by Pyrolysis of Ferrocene/Melamine Mixtures. *Appl. Phys. Lett.* **1999**, *75*, 3932–3934.
28. Trasobares, S.; Stephan, O.; Colliex, C.; Hsu, W. K.; Kroto, H. W.; Walton, D. R. M. Compartmentalized CN_x Nanotubes: Chemistry, Morphology, and Growth. *J. Chem. Phys.* **2002**, *116*, 8966–8972.
29. Glerup, M.; Steinmetz, J.; Samaille, D.; Stephan, O.; Enouz, S.; Loiseau, A.; Roth, S.; Bernier, P. Synthesis of N-Doped SWCNTs Using the Arc-Discharge Procedure. *Chem. Phys. Lett.* **2004**, *387*, 193–197.
30. Suenaga, K.; Koshino, M. Atom-by-Atom Spectroscopy at Graphene Edge. *Nature* **2010**, *468*, 1088–1090.
31. Krivanek, O. L.; Chisholm, M. F.; Nicolosi, V.; Pennycook, T. J.; Corbin, G. J.; Dellby, N.; Murfitt, M. F.; Own, C. S.; Szilagyi, Z. S.; Oxley, M. P.; Pantelides, S. T.; Pennycook, S. J. Atom-by-Atom Structural and Chemical Analysis by Annular Dark-Field Electron Microscopy. *Nature* **2010**, *464*, 571–574.
32. Huang, P. Y.; Kurasch, S.; Srivastava, A.; Skakalova, V.; Kotakoski, J.; Krasheninnikov, A. V.; Hovden, R.; Mao, Q.; Meyer, J. C.; Smet, J.; Muller, D. A.; Kaiser, U. Direct Imaging of a Two-Dimensional Silica Glass on Graphene. *Nano Lett.* **2012**, *12*, 1081–1086.
33. Banhart, F. Irradiation Effects in Carbon Nanostructures. *Rep. Prog. Phys.* **1999**, *62*, 1181.
34. Meyer, J. C.; Eder, F.; Kurasch, S.; Skakalova, V.; Kotakoski, J.; Park, H. J.; Roth, S.; Chuvilin, A.; Eyhusen, S.; Benner, G.; Krasheninnikov, A. V.; Kaiser, U. Accurate Measurement of Electron Beam Induced Displacement Cross Sections for Single-Layer Graphene. *Phys. Rev. Lett.* **2012**, *108*, 196102.
35. Kotakoski, J.; Jin, C.; Lehtinen, O.; Suenaga, K.; Krasheninnikov, A. Electron Knock-on Damage in Hexagonal Boron Nitride Monolayers. *Phys. Rev. B* **2010**, *82*, 113404.
36. Zobelli, A.; Gloter, A.; Ewels, C. P.; Seifert, G.; Colliex, C. Electron Knock-on Cross Section of Carbon and Boron Nitride Nanotubes. *Phys. Rev. B* **2007**, *75*, 245402.
37. McKinley, W. A., Jr.; Feshbach, H. The Coulomb Scattering of Relativistic Electrons by Nuclei. *Phys. Rev.* **1948**, *74*, 1759–1763.

38. Zobelli, A.; Gloter, A.; Ewels, C. P.; Colliex, C. Shaping Single Walled Nanotubes with an Electron Beam. *Phys. Rev. B* **2008**, *77*, 045410.
39. Loponen, T.; Krasheninnikov, A. V.; Kaukonen, M.; Nieminen, R. M. Nitrogen-Doped Carbon Nanotubes under Electron Irradiation Simulated with a Tight-Binding Model. *Phys. Rev. B* **2006**, *74*, 073409.
40. Kotakoski, J.; Krasheninnikov, A. V.; Kaiser, U.; Meyer, J. C. From Point Defects in Graphene to Two-Dimensional Amorphous Carbon. *Phys. Rev. Lett.* **2011**, *106*, 105505.
41. Susi, T.; Zhu, Z.; Ruiz-Soria, G.; Arenal, R.; Ayala, P.; Nasibulin, A. G.; Lin, H.; Jiang, H.; Stephan, O.; Pichler, T.; Loiseau, A.; Kauppinen, E. I. Nitrogen-Doped SWCNTs Synthesized Using Ammonia and Carbon Monoxide. *Phys. Status Solidi B* **2010**, *247*, 2726–2729.
42. Susi, T.; Kaskela, A.; Zhu, Z.; Ayala, P.; Arenal, R.; Tian, Y.; Laiho, P.; Mali, J.; Nasibulin, A. G.; Jiang, H.; Lanzani, G.; Stephan, O.; Laasonen, K.; Pichler, T.; Loiseau, A.; Kauppinen, E. I. Nitrogen-Doped Single-Walled Carbon Nanotube Thin Films Exhibiting Anomalous Sheet Resistances. *Chem. Mater.* **2011**, *23*, 2201–2208.
43. Panchakarla, L.; Subrahmanyam, K.; Saha, S.; Govindaraj, A.; Krishnamurthy, H.; Waghmare, U.; Rao, C. Synthesis, Structure, and Properties of Boron-and Nitrogen-Doped Graphene. *Adv. Mater.* **2009**, *21*, 4726–4730.
44. Sheng, Z.-H.; Shao, L.; Chen, J.-J.; Bao, W.-J.; Wang, F.-B.; Xia, X.-H. Catalyst-Free Synthesis of Nitrogen-Doped Graphene *via* Thermal Annealing Graphite Oxide with Melamine and Its Excellent Electrocatalysis. *ACS Nano* **2011**, *5*, 4350–4358.
45. Cho, Y. J.; Kim, H. S.; Baik, S. Y.; Myung, Y.; Jung, C. S.; Kim, C. H.; Park, J.; Kang, H. S. Selective Nitrogen-Doping Structure of Nanosize Graphitic Layers. *J. Phys. Chem. C* **2011**, *115*, 3737–3744.
46. Fujimoto, Y.; Saito, S. Formation, Stabilities, and Electronic Properties of Nitrogen Defects in Graphene. *Phys. Rev. B* **2011**, *84*, 245446.
47. Colliex, C. New Trends in STEM-Based Nano-EELS Analysis. *J. Electron Microsc.* **1996**, *45*, 44–50.
48. Zhao, M.; Xia, Y.; Lewis, J. P.; Zhang, R. First-Principles Calculations for Nitrogen-Containing Single-Walled Carbon Nanotubes. *J. Appl. Phys.* **2003**, *94*, 2398–2402.
49. Kotakoski, J.; Meyer, J. C.; Kurasch, S.; Santos-Cottin, D.; Kaiser, U.; Krasheninnikov, A. V. Stone-Wales-Type Transformations in Carbon Nanostructures Driven by Electron Irradiation. *Phys. Rev. B* **2011**, *83*, 245420.
50. Kotakoski, J.; Santos-Cottin, D.; Krasheninnikov, A. V. Stability of Graphene Edges under Electron Beam: Equilibrium Energetics *versus* Dynamic Effects. *ACS Nano* **2012**, *6*, 671–676.
51. Komsa, H.-P.; Kotakoski, J.; Kurasch, S.; Lehtinen, O.; Kaiser, U.; Krasheninnikov, A. V. Two-Dimensional Transition Metal Dichalcogenides under Electron Irradiation: Defect Production and Doping. *Phys. Rev. Lett.* **2012**, *109*, 035503.
52. Tewary, V. K.; Yang, B. Singular Behavior of the Debye–Waller Factor of Graphene. *Phys. Rev. B* **2009**, *79*, 125416.
53. Park, H. J.; Skákalová, V.; Meyer, J.; Lee, D. S.; Iwasaki, T.; Bumby, C.; Kaiser, U.; Roth, S. Growth and Properties of Chemically Modified Graphene. *Phys. Status Solidi B* **2010**, *247*, 2915–2919.
54. Meyer, J. C.; Kisielowski, C.; Erni, R.; Rossell, M. D.; Crommie, M. F.; Zettl, A. Direct Imaging of Lattice Atoms and Topological Defects in Graphene Membranes. *Nano Lett.* **2008**, *8*, 3582–3586.
55. Kirkland, E. J. *Advanced Computing in Electron Microscopy*; Plenum: New York, 1998.
56. Rhim, S. H.; Qi, Y.; Liu, Y.; Weinert, M.; Li, L. Formation of Nitrogen-Vacancy Complexes during Plasma-Assisted Nitrogen Doping of Epitaxial Graphene on SiC(0001). *Appl. Phys. Lett.* **2012**, *100*, 233119-5.
57. Kurasch, S.; Meyer, J. C.; Künzel, D.; Gross, A.; Kaiser, U. Simulation of Bonding Effects in Hrtem Images of Light Element Materials. *Beilstein J. Nanotechnol.* **2011**, *2*, 394–404.
58. Banhart, F.; Li, J. X.; Krasheninnikov, A. V. Carbon Nanotubes under Electron Irradiation: Stability of the Tubes and Their Action as Pipes for Atom Transport. *Phys. Rev. B* **2005**, *71*, 241408.
59. Krasheninnikov, A. V.; Banhart, F.; Li, J. X.; Foster, A. S.; Nieminen, R. M. Stability of Carbon Nanotubes under Electron Irradiation: Role of Tube Diameter and Chirality. *Phys. Rev. B* **2005**, *72*, 125428.
60. El-Barbary, A. A.; Telling, R. H.; Ewels, C. P.; Heggie, M. I.; Briddon, P. R. Structure and Energetics of the Vacancy in Graphite. *Phys. Rev. B* **2003**, *68*, 144107.
61. Krasheninnikov, A. V.; Lehtinen, P. O.; Foster, A. S.; Nieminen, R. M. Bending the Rules: Contrasting Vacancy Energetics and Migration in Graphite and Carbon Nanotubes. *Chem. Phys. Lett.* **2006**, *418*, 132–136.
62. Gan, Y.; Kotakoski, J.; Krasheninnikov, A. V.; Nordlund, K.; Banhart, F. The Diffusion of Carbon Atoms inside Carbon Nanotubes. *New J. Phys.* **2008**, *10*, 023022.
63. Kotakoski, J.; Krasheninnikov, A. V.; Nordlund, K. Energetics, Structure, and Long-Range Interaction of Vacancy-Type Defects in Carbon Nanotubes: Atomistic Simulations. *Phys. Rev. B* **2006**, *74*, 245420.
64. Arenal, R.; De la Pena, F.; Stephan, O.; Walls, M.; Tence, M.; Loiseau, A.; Colliex, C. Extending the Analysis of EELS Spectrum-Imaging Data, from Elemental to Bond Mapping in Complex Nanostructures. *Ultramicroscopy* **2008**, *109*, 32–38.
65. Kaiser, U.; Biskupek, J.; Meyer, J. C.; Leschner, J.; Lechner, L.; Rose, H.; Stöger-Pollach, M.; Khlobystov, A. N.; Hartel, P.; Müller, H.; Haider, M.; Eyhusen, S.; Benner, G. Transmission Electron Microscopy at 20 kV for Imaging and Spectroscopy. *Ultramicroscopy* **2011**, *111*, 1239–1246.
66. Pels, J. R.; Kapteijn, F.; Moulijn, J. A.; Zhu, Q.; Thomas, K. M. Evolution of Nitrogen Functionalities in Carbonaceous Materials during Pyrolysis. *Carbon* **1995**, *33*, 1641–1653.
67. Kresse, G.; Furthmüller, J. Efficiency of *Ab-Initio* Total Energy Calculations for Metals and Semiconductors Using a Plane-Wave Basis Set. *Comput. Mater. Sci.* **1996**, *6*, 15–50.
68. Kresse, G.; Furthmüller, J. Efficient Iterative Schemes for *Ab Initio* Total-Energy Calculations Using a Plane-Wave Basis Set. *Phys. Rev. B* **1996**, *54*, 11169–11186.
69. Blöchl, P. E. Projector Augmented-Wave Method. *Phys. Rev. B* **1994**, *50*, 17953.
70. Perdew, J. P.; Burke, K.; Ernzerhof, M. Generalized Gradient Approximation Made Simple. *Phys. Rev. Lett.* **1996**, *77*, 3865–3868.
71. Monkhorst, H. J.; Pack, J. D. Special Points for Brillouin-Zone Integrations. *Phys. Rev. B* **1976**, *13*, 5188–5192.
72. Blaha, P.; Schwarz, K.; Madsen, G. K. H.; Kvasnicka, D.; Luitz, J., *WIEN2k: An Augmented Plane Wave and Local Orbitals Program for Calculating Crystal Properties*; Vienna University of Technology, 2001.
73. Park, H. J.; Meyer, J.; Roth, S.; Skákalová, V. Growth and Properties of Few-Layer Graphene Prepared by Chemical Vapor Deposition. *Carbon* **2010**, *48*, 1088–1094.
74. Lin, H.; Lagoute, J.; Repain, V.; Chacon, C.; Girard, Y.; Lauret, J.-S.; Arenal, R.; Ducastelle, F.; Rousset, S.; Loiseau, A. Coupled Study by TEM/EELS and STM/STS of Electronic Properties of C- and CN_x-Nanotubes. *C. R. Phys.* **2011**, *12*, 909–920.
75. Gonzalez, D.; Nasibulin, A. G.; Shandakov, S. D.; Jiang, H.; Queipo, P.; Anisimov, A. S.; Tsuneta, T.; Kauppinen, E. I. Spontaneous Charging of Single-Walled Carbon Nanotubes: A Novel Strategy for the Selective Substrate Deposition of Individual Tubes at Ambient Temperature. *Chem. Mater.* **2006**, *18*, 5052–5057.
76. Jeanguillaume, C.; Colliex, C. Spectrum-Image: The Next Step in EELS Digital Acquisition and Processing. *Ultramicroscopy* **1989**, *28*, 252–257.